Published in IET Microwaves, Antennas & Propagation
Received on 5th December 2008
Revised on 10th April 2009
doi: 10.1049/iet-map.2008.0418

ISSN 1751-8725

Gradient-based shape optimisation of conformal array antennas

P. Jacobsson T. Rylander

Signal Processing, Signals and Systems, Chalmers University of Technology, SE-412 96 Göteborg, Sweden
E-mail: per.jacobsson@chalmers.se

Abstract: We present and test a gradient-based shape optimisation method for the minimisation of the active reflection coefficient for conformal array antennas. The goal function is an average of the active reflection coefficient with respect to all antenna elements, a prespecified frequency interval, and a set of excitation modes. The sensitivity of the goal function with respect to changes of the antenna's shape is based on the continuum form of Maxwell's equations, which provides good flexibility for the choice of field solver. The sensitivity is formulated in terms of the field solution of the original antenna problem and a similar adjoint field problem, which gives the sensitivity for an arbitrary number of design parameters given the solution of Maxwell's equations. We test the optimisation method in two dimensions for array antennas that conform to a circular cylinder, where both uniform arrays and arrays that occupy a part of the cylinder's circumference are considered. For some cases, we find that it is feasible to reduce the active reflection coefficient for arrays that partially cover the circumference of the cylinder by means of end elements that differ from the bulk elements of the array. In general, substantial reductions in the active reflection coefficient can be achieved by relatively small shape changes of the antenna elements. For the test cases considered in this article, the optimisation method typically converges to an optimised design within 5–15 iterations.

1 Introduction

Array antennas are useful for beam forming, which is achieved by controlling the excitation for each antenna element in the array. Furthermore, conformal array antennas, where the antenna conforms to some surface, are important for antenna applications where the antenna has to be integrated into an existing design. Reasons for this can be to preserve certain features of the application, for example, aerodynamic performance or aesthetic design. In addition, array antennas conforming to, for example, a cylinder can also have a beam coverage of up to 360° as opposed to planar array antennas.

An important consideration in the electromagnetic design of an array antenna is to achieve a low reflection at the aperture of the array antenna for the range of excitations that is necessary for beam-forming purposes. One important way to achieve this is to alter the geometry of the antenna elements in the array. Optimisation of the radiation efficiency with respect to the shape of a single horn has been performed in electromagnetics [1] and acoustics [2, 3]. Moreover, an analytic method for analysing the impedance for acoustic horns is presented in [4, 5]. The influence of the antenna elements' shape on the active reflection coefficient of an array antenna is an extensively studied problem, which is typically treated by means of parameter studies [6, 7]. Studies on the effects of the antenna elements' geometry on the far-field pattern have been conducted in the two-dimensional (2D) case in electromagnetics [8]. These studies indicate that the geometry of the antenna is important for the reflection of a transmitted wave. In the context of an array antenna, however, the shape of the antenna elements appears to have a limited effect on the beam-forming ability of the array antenna. Pattern synthesis by means of controlling the excitations has been thoroughly studied using genetic algorithms [9–11], simulated annealing [12], and methods based on Dolph–Chebyshev pattern synthesis [13, 14].

In this article, we present an unbiased and efficient method for the optimisation of the active reflection coefficient with respect to the shape of the antenna elements for conformal

array antennas. The optimisation method utilises accurate numerical field solvers and its goal function is expressed as an average of the active reflection coefficient with respect to the frequency interval, excitation modes of interest, and the ports of the array antenna. Our formulation is based on the continuum form of Maxwell's equations, which offers good flexibility with respect to the choice of field solver. The gradient of the goal function is expressed in terms of the solutions of the original field problem and a similar adjoint field problem [15, 16]. Consequently, the computational work is independent of the number of design parameters that are used to describe the individual antenna elements. This feature of our optimisation method offers both high computational efficiency and the possibility for a geometry description with many design parameters that can be used for complicated array antennas with many, not necessarily identical, antenna elements. We test our optimisation method on array antennas that can be modelled in 2D, where we exploit a field solver that combines the finite-difference time-domain (FDTD) scheme [17] and the finite element method (FEM) [18]. The tests feature arrays that conform to a circular cylinder. We consider both a uniform array of identical antenna elements and an array that occupies a part of the cylinder's circumference, where the elements at the ends of the array are of different shape as compared to the bulk elements. The main contributions in this article are (i) the derivation of the continuum expression for the gradient of the active reflection coefficient for shape optimisation of array antennas in three dimensions (3D), and (ii) shape optimisation of array antennas in 2D that conform to a circular cylinder.

2 Optimisation method

We consider an array antenna with N antenna elements in 3D. Each antenna element is fed by a waveguide supporting one transverse electromagnetic (TEM) mode and the frequency interval of operation is such that only the TEM mode propagates. The electric field satisfies the homogeneous vector Helmholtz equation in the domain Ω that consists of the array antenna and its surrounding environment. The boundary of Ω is denoted by $\partial\,\Omega$ and it consists of the port surfaces S_p (with $p = 0, \ldots, N-1$), the perfectly electrically conducting surfaces S_{PEC} of the array antenna and its supporting structure, and the spherical surface S_R of radius R that encloses the antenna and its supporting structure. The outward-pointing normal of Ω is denoted by $\hat{n}$.

The field at port p is described in terms of the TEM mode $\boldsymbol{m}(\xi, v)$ as $\boldsymbol{E} = V_p^+ \boldsymbol{m} e^{-jk\zeta} + V_p^- \boldsymbol{m} e^{jk\zeta}$, which gives a Robin boundary condition at S_p [18]. A Dirichlet boundary condition is applied at S_{PEC}, and at S_R the Sommerfeld radiation condition [18] is used. This field problem is formulated in weak form [18] as: find $\boldsymbol{E}$ such that

$$a(\boldsymbol{w}, \boldsymbol{E}) = b(\boldsymbol{w}) \tag{1}$$

for all test functions $\boldsymbol{w}$ that fulfil the Dirichlet boundary condition, where

$$\begin{aligned} a(\boldsymbol{w}, \boldsymbol{E}) = &\int_\Omega (\nabla \times \boldsymbol{w} \cdot \nabla \times \boldsymbol{E} - k^2 \boldsymbol{w} \cdot \boldsymbol{E}) \mathrm{d}v \\ &+ jk \sum_p \int_{S_p} (\hat{n} \times \boldsymbol{w}) \cdot (\hat{n} \times \boldsymbol{E}) \mathrm{d}s \\ &+ jk \int_{S_R} (\hat{r} \times \boldsymbol{w}) \cdot (\hat{r} \times \boldsymbol{E}) \mathrm{d}s \end{aligned} \tag{2}$$

and

$$b(\boldsymbol{w}) = \sum_p b_p(\boldsymbol{w}) = \sum_p 2jk \int_{S_p} V_p^+ \boldsymbol{m} \cdot \boldsymbol{w}\, \mathrm{d}s \tag{3}$$

2.1 Gradient of the active reflection coefficient in 3D

In this article, the objective is to minimise the active reflection coefficient [19]

$$\Gamma_p = \sum_{q=0}^{N-1} \frac{V_q^+}{V_p^+} S_{pq} \tag{4}$$

with the scattering matrix elements given by $S_{pq} = v_p^-/v_q^+ = -v_p^+/v_q^+ + Cb_p(\mathbf{E})$, where $C = (2jkv_p^+ v_q^+ \int_{S_p} |\boldsymbol{m}|^2 \mathrm{d}s)^{-1}$ and v refers to the voltages used for the computation of the scattering matrix. An expression for the first-order variation of the active reflection coefficient with respect to geometry perturbations is formulated in terms of the solution of the original field problem and an adjoint field problem. Given that the geometry of the feeding waveguides is unperturbed, we express the variation of S_{pq} as $\delta S_{pq} = Cb_p(\delta \boldsymbol{E})$ and formulate an adjoint problem $a(\tilde{\boldsymbol{E}}, \boldsymbol{w}) = b_p(\boldsymbol{w})$, where $\tilde{\boldsymbol{E}}$ is the solution to the adjoint problem. The variation of the scattering matrix is expressed as [16]

$$\begin{aligned} \delta S_{pq} &= Cb_p(\delta \boldsymbol{E}) = Ca(\tilde{\boldsymbol{E}}, \delta \boldsymbol{E}) \\ &= -C\delta a(\boldsymbol{E}, \tilde{\boldsymbol{E}}) \\ &= -C \int_S (\nabla \times \boldsymbol{E} \cdot \nabla \times \tilde{\boldsymbol{E}} - k^2 \boldsymbol{E} \cdot \tilde{\boldsymbol{E}}) \delta\gamma \mathrm{d}s \end{aligned} \tag{5}$$

where $\boldsymbol{E}$ is the solution to the original problem when port q is excited and $\tilde{\boldsymbol{E}}$ is the solution to the adjoint problem when port p is excited. In (5), $\delta\gamma$ is a small normal displacement of the boundary of the array antenna, where $\delta\gamma < 0$ for perturbations in the direction of $\hat{n}$. The sensitivity of the active reflection coefficient is

$$\begin{aligned} \delta\Gamma_p = \sum_{q=0}^{N-1} \frac{V_q^+}{V_p^+} \delta S_{pq} = -\sum_{q=0}^{N-1} \Bigg(&\frac{V_q^+}{V_p^+} \frac{1}{2jkv_p^+ v_q^+ \int_{S_P} |\boldsymbol{m}|^2 \mathrm{d}s} \\ &\times \int_S (\nabla \times \boldsymbol{E} \cdot \nabla \times \tilde{\boldsymbol{E}} - k^2 \boldsymbol{E} \cdot \tilde{\boldsymbol{E}}) \delta\gamma \mathrm{d}s \Bigg) \end{aligned} \tag{6}$$

2.2 Gradient of the active reflection coefficient in 2D

For testing purposes, we consider shape optimisation of array antennas that can be described by an infinitely long cylinder, where the excitation of the array antenna yields a transverse electric field with respect to the cylinder axis. In particular, we consider shape optimisation for array antennas conforming to a circular cylinder as shown in Fig. 1. Fig. 2 shows the geometry description for antenna element p, where each side of the horn is described by a Bézier curve of degree three that features four control points. The horns are fed by parallel plate waveguides of length l_w and width w_w, which are chosen such that only the fundamental TEM mode is significant at the port.

For circular arrays, it is useful to consider phase mode excitations $V_p^+ = \tilde{V}_m e^{jm\varphi_p}$, where $\tilde{V}_m$ is the phase mode amplitude. The angle φ_p is the azimuthal angle with respect to the x-axis such that $\varphi_p = p\Delta\varphi$, where $\Delta\varphi = 2\pi/N$, and $p = 0, \ldots, N-1$ is the port number. To characterise the performance of the array antenna, we use the active reflection coefficient (4) which can be stated in terms of phase modes as

$$\tilde{\Gamma}_p^m = \sum_{q=0}^{N-1} e^{jm\Delta\varphi(q-p)} S_{pq} \tag{7}$$

In the general case, the active reflection coefficient is different for each antenna element, but for a uniform array antenna with identical antenna elements, $\tilde{\Gamma}_p^m$ is independent of p. The variation of the active reflection coefficient is expressed as

$$\delta\tilde{\Gamma}_p^m = \sum_{q=0}^{N-1} \delta S_{pq} e^{jm(q-p)\Delta\varphi} = -\sum_{q=0}^{N-1} \left(\frac{w_w e^{jm(q-p)\Delta\varphi}}{2jkv_p^+ v_q^+} \times \int_L (\nabla \times \boldsymbol{E} \cdot \nabla \times \tilde{\boldsymbol{E}} - k^2 \boldsymbol{E} \cdot \tilde{\boldsymbol{E}}) \delta\gamma \, dl \right) \tag{8}$$

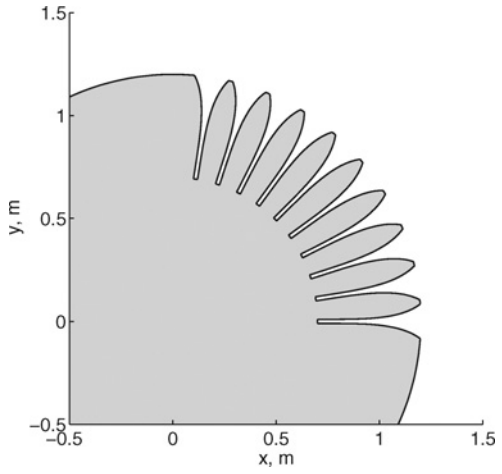

Figure 1 *Array with antenna elements conforming to a circular cylinder*

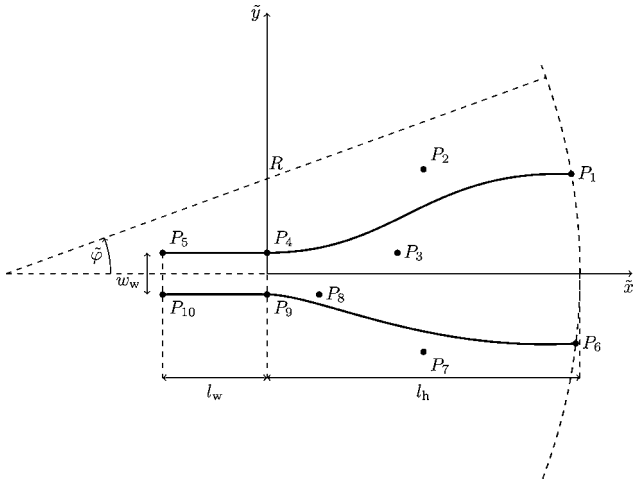

Figure 2 *The horn geometry consists of a waveguide part and a horn part described by two Bézier curves with four control points each, that is, $P_1, \ldots, P_4$ and $P_6, \ldots, P_9$*
The horn geometry is specified in terms of local coordinates $\tilde{x}$ and $\tilde{y}$

From (8) it is clear that the active reflection coefficient and its gradient with respect to geometry perturbations can be calculated by solving N field problems. In the case of a uniform array with identical antenna elements, it is sufficient to solve a single field problem to calculate the goal function and its gradient with respect to geometry perturbations.

3 Numerical tests

We minimise the root-mean-square (RMS) value of the active reflection coefficient for a frequency interval $[f_{min}, f_{max}]$, all the N ports, and a set of excitation modes $\mathcal{M} = \{m_1, \ldots, m_M\}$. Thus, the goal function is given by

$$g = \left[\frac{1}{M} \sum_{m \in \mathcal{M}} \frac{1}{N} \sum_{p=0}^{N-1} \left(\frac{1}{f_{max} - f_{min}} \int_{f_{min}}^{f_{max}} |\tilde{\Gamma}_p^m|^2 \, df \right) \right]^{1/2} \tag{9}$$

The overall size of the array ($R = 1.2$ m), the number of horns (N), the waveguide dimensions ($w_w = 0.02$ m, $l_w = 0.1$ m), and the length of the horn ($l_h = 0.4$ or 0.8 m) are fixed in the optimisation. The design parameters for each horn are the local coordinates $\tilde{y}_1, \tilde{x}_2, \tilde{y}_2, \tilde{x}_3, \tilde{y}_6, \tilde{x}_7, \tilde{y}_7, \tilde{x}_8$, where $P_i = (\tilde{x}_i, \tilde{y}_i)$ in Fig. 2 and

$$0 < \tilde{\varphi}_1 < \frac{d}{2R} \tag{10}$$

$$\tilde{x}_1 - \frac{l_h}{2} < \tilde{x}_2 < \tilde{x}_1 \tag{11}$$

$$0 < \tilde{y}_2 < R \cos \frac{d}{2R} \tag{12}$$

$$0 < \tilde{x}_3 < \frac{l_h}{2} \tag{13}$$

and similarly for the other design parameters. The remaining coordinates of the control points are fixed to enforce

doi: 10.1049/iet-map.2008.0418

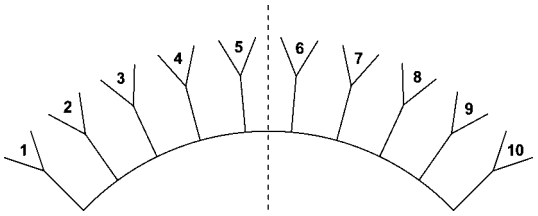

Figure 3 *Schematic picture of the finite array antenna with ten numbered antenna elements*

The dashed line indicates the symmetry line of the array

continuity of the horn's geometry and its derivatives. Thus, the maximum number of design parameters for the array antenna is $8N$, which is restricted by constraints as described below.

Linear constraints can be used in the optimisation algorithm to enforce symmetries of the array in a straightforward manner and we investigate two basic cases: (i) a uniform array with 40 antenna elements distributed over the entire circumference of the circular cylinder, where all antenna elements are identical and described by the four-parameter vector $\boldsymbol{B}$; and (ii) an array with 10 elements distributed over a part of the circumference of the circular cylinder. In the following, the array that only partially covers the circumference of the circular cylinder is referred to as a finite array since it features end elements at the two ends of the array. We use the element separation $d = 2\ \pi\ R/N$ for the uniform array with $N = 40$ and this value for d is also used for the finite array. The finite array, schematically depicted in Fig. 3, is tested with four different constraints on the antenna elements at the ends of the array. Table 1 shows the geometries and the parameters which describe each individual horn in terms of the four-parameter vectors $\boldsymbol{B}$, $\boldsymbol{S}$, $\boldsymbol{S}_1$, $\boldsymbol{S}_2$, and the eight-parameter vector $\boldsymbol{A}$. The geometry $\mathcal{E}$ consists of identical symmetric antenna elements described by $\boldsymbol{B}$. The second geometry, $\mathcal{S}_1$, consists of the identical and symmetric bulk horns 2–9 described by $\boldsymbol{B}$ and the symmetric horns 1 and 10 described by $\boldsymbol{S}$. The third geometry, $\mathcal{S}_2$, consists of the identical symmetric bulk horns 3–8 described by $\boldsymbol{B}$, the symmetric horns 1 and 10 described by $\boldsymbol{S}_1$, and the symmetric horns 2 and 9 described by $\boldsymbol{S}_2$. The fourth geometry consists of the symmetric bulk horns 2–9 described by $\boldsymbol{B}$ and the asymmetric horns 1 and 10 described by $\boldsymbol{A}$. Thus, geometry $\mathcal{E}$ is described by four degrees of freedom, $\mathcal{S}_1$ by eight degrees of freedom, and $\mathcal{S}_2$ and $\mathcal{A}_1$ by 12 degrees of freedom.

The field problem is solved by a stable FEM–FDTD hybrid method [20] formulated in the time domain. It combines the efficiency of the FDTD scheme in large homogeneous regions outside the array antenna with the body-conforming ability of the FEM in the vicinity of the curved boundary of the array antenna. In the numerical simulations, we use a resolution of 20 cells per wavelength at the highest frequency and truncate the computational domain by a perfectly matched layer [17]. The use of a time-domain method allows us to compute the frequency-domain solution for a given frequency range by the Fourier transform of the time-domain solution. For the optimisation, we use sequential quadratic programming implemented by the routine NPSOL [21]. This optimisation routine is part of a larger package of optimisation algorithms provided by TOMLAB.

3.1 Uniform array antenna

The active reflection coefficient as a function of frequency for an initial and optimised design of the uniform array is shown in Fig. 4, where the optimisation is performed for $m = 0$ and the frequency interval 796–955 MHz that corresponds to $0.5 \leq d/\lambda \leq 0.6$. (This frequency interval is indicated by the shaded area in the figure.) The dashed line in the figure refers to the initial array and the solid line to the optimised array. The active reflection coefficient is significantly reduced for the frequency interval and the goal-function value is reduced from 0.11 to 0.02 in seven iterations, which amounts to a total of 16 solutions of the field problem including minor iterations, that is, line searches.

Fig. 5 shows the shape of the initial horn (dashed line) together with the shape of the optimised horn (solid line). A relatively small change in the geometry of the horn results in a significant change in the active reflection coefficient, which makes shape optimisation a well-suited tool for the design of array antennas.

Given the ith antenna element in the array, its neighbouring antenna elements are important for the reduction of the active reflection coefficient. Fig. 6 shows the self-reflection $|S_{ii}|$ for the ith horn (solid line) together with $|\sum_{j=i-1}^{i+1} S_{ij}|$

Table 1 Four finite array geometries $\mathcal{E}$, $\mathcal{S}_1$, $\mathcal{S}_2$, and $\mathcal{A}_1$ described by the four-parameter vectors $\boldsymbol{B}$, $\boldsymbol{S}$, $\boldsymbol{S}_1$, $\boldsymbol{S}_2$, and the eight-parameter vector $\boldsymbol{A}$. The numbering of the antenna elements is shown in Fig. 3

	Antenna element index									
	1	2	3	4	5	6	7	8	9	10
$\mathcal{E}$	$\boldsymbol{B}$	$\boldsymbol{B}$	$\boldsymbol{B}$	$\boldsymbol{B}$	$\boldsymbol{B}$	$\boldsymbol{B}$	$\boldsymbol{B}$	$\boldsymbol{B}$	$\boldsymbol{B}$	$\boldsymbol{B}$
$\mathcal{S}_1$	$\boldsymbol{S}$	$\boldsymbol{B}$	$\boldsymbol{B}$	$\boldsymbol{B}$	$\boldsymbol{B}$	$\boldsymbol{B}$	$\boldsymbol{B}$	$\boldsymbol{B}$	$\boldsymbol{B}$	$\boldsymbol{S}$
$\mathcal{S}_2$	$\boldsymbol{S}_1$	$\boldsymbol{S}_2$	$\boldsymbol{B}$	$\boldsymbol{B}$	$\boldsymbol{B}$	$\boldsymbol{B}$	$\boldsymbol{B}$	$\boldsymbol{B}$	$\boldsymbol{S}_2$	$\boldsymbol{S}_1$
$\mathcal{A}_1$	$\boldsymbol{A}$	$\boldsymbol{B}$	$\boldsymbol{B}$	$\boldsymbol{B}$	$\boldsymbol{B}$	$\boldsymbol{B}$	$\boldsymbol{B}$	$\boldsymbol{B}$	$\boldsymbol{B}$	$\boldsymbol{A}$

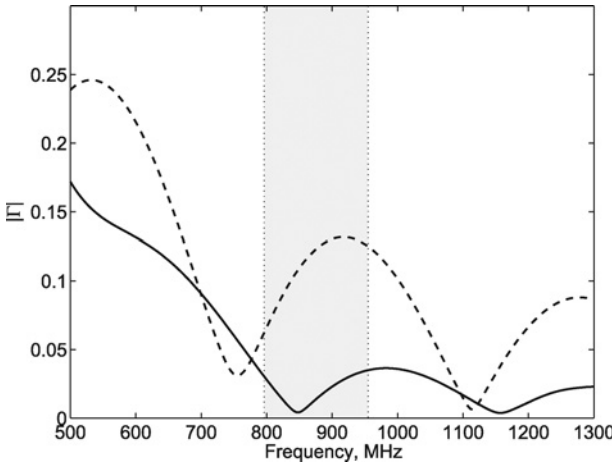

Figure 4 *Active reflection coefficient as a function of frequency for the initial geometry (dashed line) and the optimised geometry (solid line) for a uniform array*

The optimisation is performed for the frequency interval 796–955 MHz (shown by the shaded area) and uniform excitation $m = 0$

that includes contributions from the two neighbouring horns (dash-dotted line) and $|\sum_{j=i-2}^{i+2} S_{ij}|$ that includes contributions from the four neighbouring horns (dotted line). For the lowest mode, $m = 0$, the active reflection coefficient for horn i is the sum of the ith row in the scattering matrix and it is also shown in Fig. 6 (dashed line). Although the self-reflection $|S_{ii}|$ is relatively large, the contributions from the other elements reduce the active reflection coefficient efficiently and the four adjacent elements provide the main contribution.

The uniform array is compared to a single antenna element placed on the circular cylinder, cf. [2, 3]. Fig. 7 shows the shape of the optimised single horn for the frequency interval 796–955 MHz and it is noted that this design is rather different as compared to the optimised design shown in Fig. 5. The reflection coefficient $|\tilde{S}_{11}|$ for the single horn is significantly lower than the self-reflection $|S_{ii}|$ for the horns in the uniform array as shown in Fig. 8: $|S_{ii}|$ for a

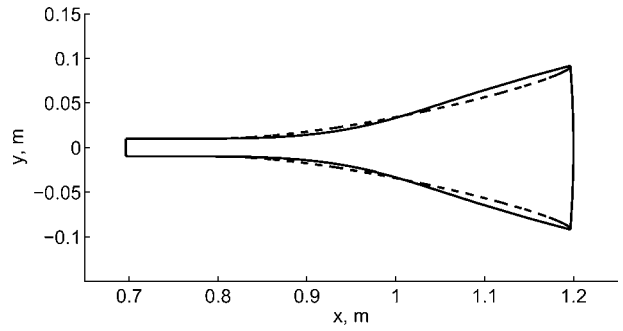

Figure 5 *Initial shape of the horn (dashed line) and the optimised shape of the horn (solid line) for a uniform array*

The optimisation is performed for the frequency interval 796–955 MHz and uniform excitation $m = 0$

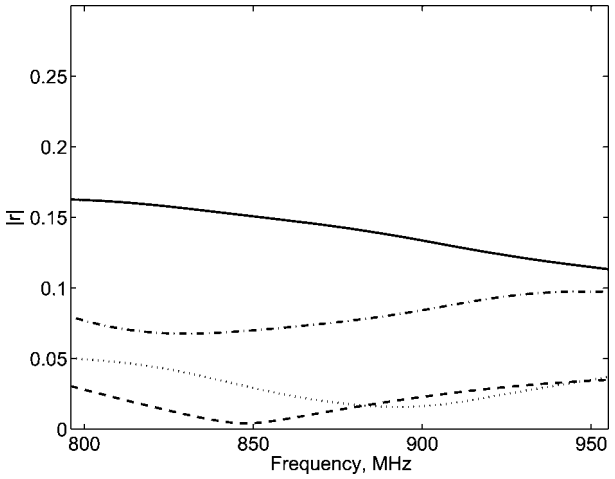

Figure 6 *Contributions $|r|$ to the active reflection coefficient of an optimised uniform array for the horn with index i: $r = S_{ii}$ – solid line; $r = S_{ii} + S_{i,i-1} + S_{i,i+1}$ – dash-dotted line; $r = S_{ii} + S_{i,i-2} + S_{i,i-1} + S_{i,i+1} + S_{i,i+2}$ – dotted line; and $r = \sum_j S_{ij}$ – dashed line*

The optimisation is performed for the frequency interval 796–955 MHz and uniform excitation $m = 0$

horn in the uniform array – solid line; $|\tilde{S}_{11}|$ for the single horn – dashed line; and the active reflection coefficient $|\sum_{j=1}^{N} S_{ij}|$ for the uniform array – dash-dotted line. A uniform array antenna with identical horns of the shape shown in Fig. 7 has an active reflection coefficient that is an order of magnitude larger than a uniform array consisting of horns with the optimised shape shown in Fig. 5. Therefore it is important to optimise the entire array, which advocates the use of the optimisation and numerical techniques proposed in this paper as design tools.

3.2 Array antennas with end effects

In this section, we optimise the finite array antennas with the configuration of end elements described in Table 1. When the antenna elements do not cover the entire circumference of the cylinder, the array is no longer uniform and each antenna element experiences a different electromagnetic

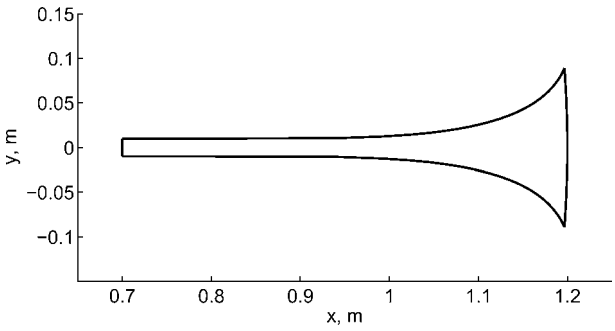

Figure 7 *Optimised shape of a single horn integrated in a circular cylinder*

The optimisation is performed for the frequency interval 796–955 MHz

doi: 10.1049/iet-map.2008.0418

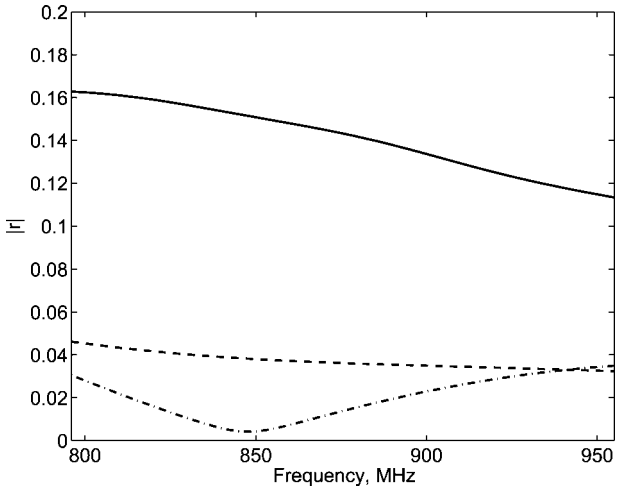

Figure 8 *Reflection coefficient |r| for: a horn with index i in a uniform array ($r = S_{ii}$) – solid line; and a single horn array ($r = \tilde{S}_{11}$) – dashed line*

The active reflection coefficient for the uniform array is also shown ($r = \Sigma_{j=1}^{N} S_{ij}$) – dash-dotted line. The optimisation is performed for the frequency interval 796–955 MHz

environment. In particular, the horns at the ends of the array only have other antenna elements on one side but not the other side, which yields an environment quite different from the bulk elements in the middle of the array. Numerical tests show that it is in some cases advantageous to introduce extra degrees of freedom for the end elements, but that it suffices to let all the bulk horns be identical and symmetric. This conclusion is also supported by the results on mutual coupling discussed in Section 3.1.

3.2.1 Asymmetric end elements: The array with asymmetric end elements labelled $\mathcal{A}_1$ in Table 1 yields in general the best results (as compared to the other types of end elements considered here) and we explore the optimisation of this type of array first. In Fig. 9, the optimised horn geometry for the bulk horn (dash-dotted line) and the end element 10 (dashed line) are shown together with the previous results for the uniform array (solid line), where the optimisation is performed for $m = 0$ and the frequency interval 796–955 MHz that corresponds to $0.5 \leq d / \lambda \leq 0.6$. The bulk horns of the finite array are very similar to the horns for the uniform array, whereas the elements at the end of the finite array are distinctively different from the bulk elements. The initial geometry is identical for all antenna elements and the initial value of the goal function (9) is 0.11. The goal function value for the optimised finite array is 0.03, which can be compared to the goal function value 0.02 for the optimised uniform array discussed in Section 3.1.

Furthermore, we compare the optimised finite array (geometry $\mathcal{A}_1$) for $m = 0$ and two different frequency intervals: (i) 478–637 MHz, where $0.3 \leq d / \lambda \leq 0.4$ and (ii) 796–955 MHz, where $0.5 \leq d / \lambda \leq 0.6$. The optimised shapes for the lower (dashed line) and higher (solid line) frequency interval are shown in Fig. 10 and the corresponding active reflection coefficients as a function of frequency are shown in Fig. 11. For optimisation with respect to the higher frequency interval, the optimised design features relatively straight edges that are joined with the feeding waveguide by a curved shape in the region $0.8 \leq x \leq 0.95$, as shown in Fig. 10. This geometry yields a low active reflection coefficient for the frequency interval that corresponds to $0.5 \leq d/\lambda \leq 0.6$ at the expense of a rather large active reflection coefficient for $0.3 \leq d/\lambda \leq 0.4$. For optimisation with respect to the lower frequency interval, the region with a curved boundary is increased to $0.8 \leq x \leq 1.1$ and a considerably smaller section next to the aperture features relatively straight edges. This design yields a significantly lower active reflection coefficient for $0.3 \leq d/\lambda \leq 0.4$ at the cost of a relatively small increase for $0.5 \leq d/\lambda \leq 0.6$. Shin and Schaubert [6] performed a parameter study of stripline-fed Vivaldi notch-antenna arrays and they found similar dependencies on their opening rate parameter R, which corresponds to a linear tapering in the limiting case $R \to 0$ and exponential tapering for $R > 0$ for the full length of the antenna element's tapered slot. (Our optimisation method allows for combinations of curved and straight boundaries, which is

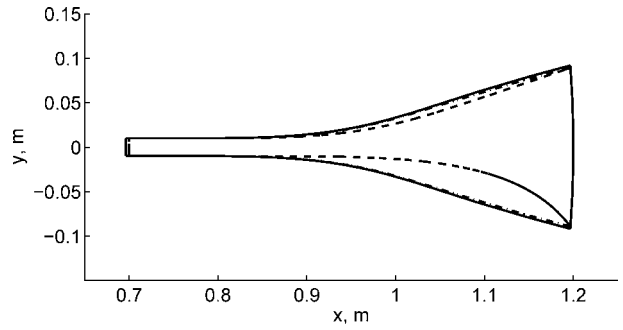

Figure 9 *Horn geometry for a uniform array (solid line) shown together with the bulk horn (dash-dotted line) and edge horn (dashed line) of a finite array, where the optimisation is performed for $m = 0$ and the frequency interval 796–955 MHz that corresponds to $0.5 \leq d / \lambda \leq 0.6$*

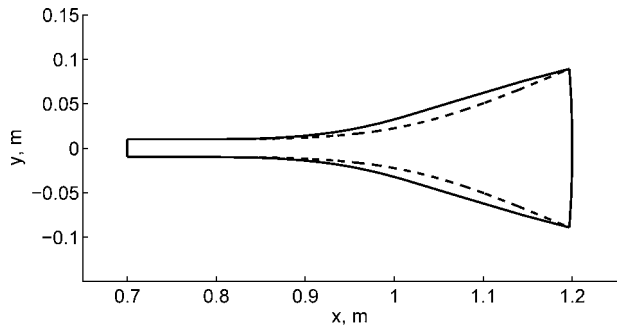

Figure 10 *Optimised shapes of the bulk horns for a finite array for $m = 0$*

Shapes are shown for the frequency interval 478–637 MHz (dashed line) and 796–955 MHz (solid line). The corresponding active reflection coefficients are shown in Fig. 11

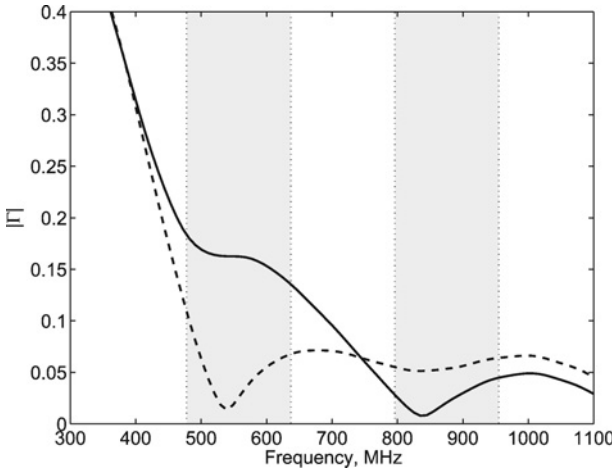

Figure 11 *Active reflection coefficient as a function of frequency for the optimised shapes shown in Fig. 10, that is, optimised shapes for m = 0 and the frequency interval 478–637 MHz (dashed line) and 796–955 MHz (solid line)*
The two frequency intervals are indicated by shaded areas

displayed by the optimised designs shown in Fig. 10 given the parameterisation that we use here.) In particular, Shin and Schaubert [6] show improved standing wave ratios at low frequencies when R is increased, which compares well with our shapes optimised for the lower frequency interval and the corresponding active reflection coefficient.

Furthermore, Shin and Schaubert [6] also find that it is advantageous to have a large aperture opening in combination with a small taper flare angle close to the feed of the antenna elements, which also agrees well with the optimised designs that we find. In fact, the constraint on the maximum aperture opening that we use is active (or very close to active) for all our optimised designs. Finally, we increase the length of the horns by a factor of two such that $l_h = 0.8$ m, where the parameterisation of the boundary remains the same. (The optimisation of longer antenna elements may benefit from additional design parameters that allow for greater geometrical flexibility, but we find that a Bézier curve of degree three suffices to demonstrate the main features of our optimisation method.) Fig. 12 shows the optimised bulk horn for geometry $\mathcal{A}_1$ by a solid curve when the goal function averages over the frequency interval that corresponds to $0.3 \leq d/\lambda \leq 0.4$ given a uniform excitation, that is, $m = 0$. Clearly, this design features mainly flat boundaries and we achieve very similar results for the optimisation when $0.5 \leq d/\lambda \leq 0.6$. For higher mode numbers $|m|$, the field variations in the radial direction are reduced, which may be interpreted as a decrease in the radial component of the wave vector. As a result, the field variation perpendicular to the array aperture is reduced which may make it more challenging to find designs that yield good impedance transitions from the waveguides to free space. We find that such situations yield optimised designs that feature curved boundaries to a greater extent. Fig. 12 shows the shape of an optimised design for $m = 2$ and $0.3 \leq d/\lambda \leq 0.4$ (dashed curve), which clearly differs from the case when $m = 0$. We find similar optimised shapes for $0.5 \leq d/\lambda \leq 0.6$, although the curved boundaries are less pronounced for the higher frequency interval.

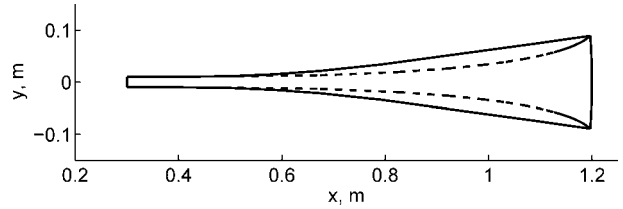

Figure 12 *Optimised shape for long horns for the frequency interval 478–637 MHz and m = 0 (solid line) and m = 2 (dashed line)*

3.2.2 Comparison of different end elements:

Table 2 shows the RMS value of the active reflection coefficient with respect to frequency for each antenna element in the finite array, where the optimisation is performed for the frequency range 796–955 MHz and $m = 0$. The first column shows the RMS value when all horns in the array are identical (geometry $\mathcal{E}$) and the second column shows the RMS value when the edge horns are allowed to be different from the bulk horns and asymmetric (geometry $\mathcal{A}_1$). The table shows that the RMS value of the active reflection coefficient for the elements at the ends of the array are significantly reduced when they are allowed to be asymmetric. (Only the result for horns 1–5 in Fig. 3 are shown because of the symmetry.) This result indicates that it is feasible to exploit also the end elements in a finite array to achieve an improved active reflection coefficient. Thus, it would be possible to avoid so-called dummy elements to truncate finite arrays – a design solution that is often used in practice and is considered expensive.

Since the shape of the antenna elements at the ends of the finite array has a significant effect on the active reflection coefficient, we investigate different constraints for the horns at the ends of the array. The four geometries $\mathcal{E}$, $\mathcal{S}_1$, $\mathcal{S}_2$ and $\mathcal{A}_1$ described in Table 1 are considered. The goal function

Table 2 RMS value of the active reflection coefficient for the horns 1–5 in a finite array with ten antenna elements for the geometries $\mathcal{E}$ and $\mathcal{A}_1$

Horn	$\mathcal{E}$	$\mathcal{A}_1$
1	0.060	0.009
2	0.056	0.045
3	0.018	0.018
4	0.031	0.031
5	0.025	0.024

doi: 10.1049/iet-map.2008.0418

Table 3 Goal function values for different combinations of horn length, frequency range, mode number and constraints on the horns at the two ends of the finite array antenna with ten antenna elements

Constraint	$l_h = 0.4$ m				$l_h = 0.8$ m			
	478–637 MHz		796–955 MHz		478–637 MHz		796–955 MHz	
	$m = 0$	$m = 2$	$m = 0$	$m = 2$	$m = 0$	$m = 2$	$m = 0$	$m = 2$
$\mathcal{E}$	0.079	0.102	0.043	0.052	0.051	0.071	0.035	0.054
$\mathcal{S}_1$	0.057	0.096	0.035	0.049	0.035	0.071	0.029	0.053
$\mathcal{S}_2$	0.052	0.093	0.034	0.049	0.035	0.070	0.028	0.053
$\mathcal{A}_1$	0.057	0.087	0.030	0.049	0.035	0.069	0.027	0.053

for the optimised designs are shown in Table 3 for various situations: frequency range 478–637 MHz and 796–955 MHz; mode $m = 0$ and 2; and horn length $l_h = 0.4$ and 0.8 m. In most cases, the goal function takes its lowest value for the configuration with asymmetric edge horns. Furthermore, the longer horns with $l_h = 0.8$ m yield a lower value of the goal function for most cases, and the reduction is largest for the lower frequency band. It should be emphasised that the same parameterisation is used for both the long and the short horns, which effectively may put the long horns at a disadvantage with respect to geometrical flexibility. However, this test demonstrates that the optimisation method proposed in this article yields designs with low active reflection coefficient for approximately 5–15 iterations, where further reductions may be achieved if more flexible geometry descriptions and more design parameters are used. Finally, the higher-order modes yield in general a larger value of the goal function.

3.2.3 Optimisation for all excitation modes:

Electronically controlled beam forming is an important application for array antennas. For such situations, it is typically desirable to use the M lowest excitation modes and, consequently, find array antenna designs that yield an active reflection coefficient that is low on average for these modes given the frequency band of interest. For geometry $\mathcal{A}_1$, we perform the optimisation with all radiating modes [19] included in the goal function (9). For the frequency range 796–955 MHz, all the modes $m = 0, \pm1, \pm2, \pm3, \pm4, 5$ radiate. Thus, we include in the goal function (9) all the ten modes that are feasible for the finite array antenna with $N = 10$ antenna elements.

Fig. 13 shows the optimised shape of the bulk horn (solid line) together with the optimised shape of the antenna element 10 (dashed line) at the end of the finite array. Here, the goal function features a compromise with respect to a range of excitations and it clearly influences the optimised shapes of the antenna elements, where the end elements are particularly affected as compared to the optimised designs in Section 3.2.1. The active reflection coefficient as a function of frequency for the optimised array is shown in Fig. 14 for the individual modes by solid

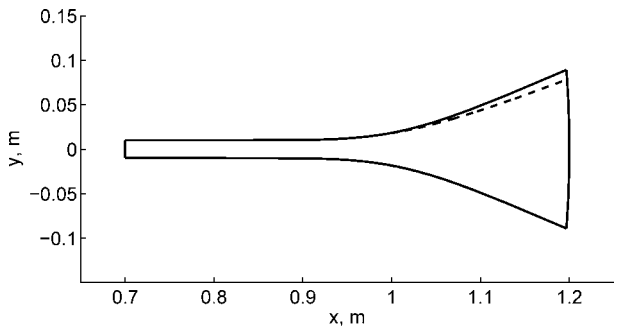

Figure 13 *Optimised horn shape for the bulk horns (solid line) and antenna element 10 (dashed line) for the finite array $\mathcal{A}_1$ when all modes are included in the goal function*

The optimisation is performed for the frequency interval 796–955 MHz

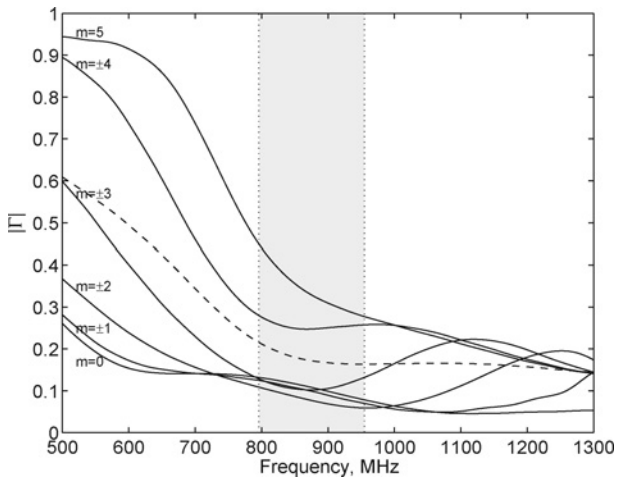

Figure 14 *Active reflection coefficient for all modes for a finite array $\mathcal{A}_1$ with the horn shape shown in Fig. 13*

The dashed line shows the RMS of the active reflection coefficient with respect to all modes. The shaded area indicates the frequency interval (796–955 MHz) considered in the optimisation

curves, where each curve is the RMS average for the ten ports. It is noted that the higher modes typically yield a larger reflection. Fig. 14 also shows the average of the active reflection coefficient with respect to both the ports and the modes by the dashed curve. We conclude that the optimisation method proposed in this paper allows for automatic and unbiased design of array antennas based on accurate field computations. If desired, goal function (9) can also be modified to include weighting factors that put emphasis on specific ports, excitation modes and/or parts of the frequency interval under consideration.

4 Conclusion

In this article, we derive the gradient of the active reflection coefficient with respect to geometry changes for an array antenna in 3D. Our derivation is based on the continuum form of Maxwell's equations and it expresses the gradient in terms of the solution of the original field problem and an adjoint field problem which renders the computational cost independent of the number of design parameters that are used to describe the geometry of the array antenna. This feature of our method also offers good flexibility with respect to the choice of field solver. The gradient is tested for a 2D array antenna conforming to a circular cylinder, where we minimise the average of the active reflection coefficient with respect to the ports, a given frequency interval and a set of excitation modes that are useful for beam-forming. The tests show that we can obtain a significant reduction in the active reflection coefficient in approximately 5–15 iterations.

We observe that relatively small changes in the geometry of the antenna can result in large changes in the active reflection coefficient. In addition, mutual coupling between the individual antenna elements is important in reducing the active reflection coefficient. These observations indicate that our optimisation method together with an efficient numerical field solver is a good tool for design of array antennas. Moreover, the antenna elements near the ends of a finite array are allowed to differ in shape from the antenna elements in the bulk of the array which may be important in order to further reduce the average active reflection coefficient.

A natural extension of this work is to test the outlined optimisation procedure for 3D array antennas. For real-world applications, it is also interesting to investigate array antennas conforming to arbitrary geometries. We conclude that our optimisation method allows for an automatised, unbiased, and efficient design procedure of complicated array antennas.

5 Acknowledgments

This work was mainly supported by the Strategic Research Center CHARMANT, financed by the Swedish Foundation for Strategic Research. Thomas Rylander was also supported in part by a mobility grant from the Swedish Foundation for Strategic Research.

6 References

[1] DEGUCHI H., TSUJI M., SHIGESAWA H.: 'Compact low-cross-polarization horn antennas with serpentine-shaped taper', *IEEE. Trans. Antennas. Propag.*, 2004, **52**, pp. 2510–2516

[2] BÄNGTSSON E., NORELAND D., BERGGREN M.: 'Shape optimization of an acoustic horn', *Comput. Methods Appl. Mech. Eng.*, 2003, **192**, pp. 1533–1671

[3] UDAWALPOLA R., BERGGREN M.: 'Optimization of an acoustic horn with respect to efficiency and directivity', *Int. J. Numer. Methods Eng.*, 2008, **73**, pp. 1571–1606

[4] PAGNEUX V., AMIR N., KERGOMARD J.: 'A study of wave propagation in varying cross-section waveguides by modal decomposition. Part I. Theory and validation', *J. Acoust. Soc. Am.*, 1996, **100**, pp. 2034–2048

[5] AMIR N., PAGNEUX V., KERGOMARD J.: 'A study of wave propagation in varying cross-section waveguides by modal decomposition. Part II. Results', *J. Acoust. Soc. Am.*, 1997, **101**, pp. 2504–2517

[6] SHIN J., SCHAUBERT D.H.: 'A parameter study of stripline-fed Vivaldi notch-antenna arrays', *IEEE. Trans. Antennas. Propag.*, 1999, **47**, pp. 879–886

[7] CHIO T.-H., SCHAUBERT D.H.: 'Parameter study and design of wide-band widescan dual-polarized tapered slot antenna arrays', *IEEE. Trans. Antennas. Propag.*, 2000, **48**, pp. 879–886

[8] HALLERÖD T., RYLANDER T.: 'Shape and excitation optimization for conformal array antennas', *Radio Sci.*, 2008, **43**, RS4011

[9] ALLARD R.J., WERNER D.H., WERNER P.L.: 'Radiation pattern synthesis for arrays of conformal antennas mounted on arbitrarily-shaped three-dimensional platforms using genetic algorithms', *IEEE. Trans. Antennas. Propag.*, 2003, **51**, pp. 1054–1062

[10] YAN K.-K., LU Y.: 'Sidelobe reduction in array-pattern synthesis using genetic algorithm', *IEEE. Trans. Antennas. Propag.*, 1997, **45**, pp. 1117–1122

[11] VIRGA K.L., ZHANG H.: 'Spatial beamformer weighting sets for circular array STAP', IEEE Int. Symp. Phased Array Systems and Technology, 2000, pp. 561–564

[12] FERREIRA J.A., ARES F.: 'Synthesis of conformal arrays by the simulated annealing technique', *Electron. Lett.*, 1997, **33**, pp. 1187–1189

doi: 10.1049/iet-map.2008.0418

[13] LAU B.K., LEUNG Y.H.: 'A Dolph-Chebyshev approach to the synthesis of array patterns for uniform circular arrays', *IEEE Int. Symp. Circuits Systems*, 2000, **1**, pp. 124–127

[14] VESCOVO R.: 'An extension of the Dolph-Chebyshev synthesis technique to circular arrays of antennas', *Int. J. Infrared Millimeter Waves*, 1999, **20**, pp. 1957–1976

[15] PIRONNEAU O.: 'Optimal Shape Design for Elliptic Systems' (Springer, 1984)

[16] BONDESON A., YANG Y., WEINERFELT P.: 'Shape optimization for radar cross sections by a gradient method', *Int. J. Numer. Methods Eng.*, 2004, **61**, (3), pp. 687–715

[17] TAFLOVE A., HAGNESS S.C.: 'Computational electrodynamics: the finite-difference time-domain method' (Artech House, 2005, 3rd edn.)

[18] JIN J.: 'The finite element method in electromagnetics' (Wiley, 2002, 2nd edn.)

[19] JOSEFSSON L., PERSSON P.: 'Conformal array antenna theory and design' (Wiley, 2006)

[20] RYLANDER T., BONDESON A.: 'Stability of explicit-implicit hybrid time-stepping schemes for Maxwell's equations', *J. Comput. Phys.*, 2002, **179**, (2), pp. 426–438

[21] GILL P.E., MURRAY W., SAUNDERS M.A., WRIGHT M.H.: 'User's guide for NPSOL 5.0: a Fortran package for nonlinear programming'. Technical Report SOL 86-2, revised July 30, Technical Report, Systems Optimization Laboratory, Department of Operations Research, Stanford University, Stanford, California 94305-4022, 1998